Data-Centric Engineering (2020), 1–**??**
doi:10.1017/dce.2020.7

CAMBRIDGE UNIVERSITY PRESS

RESEARCH ARTICLE

Supplementary material: emulating computer experiments of transport infrastructure slope stability using Gaussian processes and Bayesian inference

Aleksandra Svalova[1*], Peter Helm[2], Dennis Prangle[1], Mohamed Rouainia[2], Stephanie Glendinning[2] and Darren J Wilkinson[1]

[1]School of Mathematics, Statistics and Physics, Newcastle University, Newcastle upon Tyne, NE1 7RU, UK
[2]School of Engineering, Newcastle University, Newcastle upon Tyne, NR1 7RU, UK
*Corresponding author. E-mail: alex.svalova@newcastle.ac.uk

Received: June 30, 2021; **Revised:** NA; **Accepted:** NA

Geotechnical model geometry array

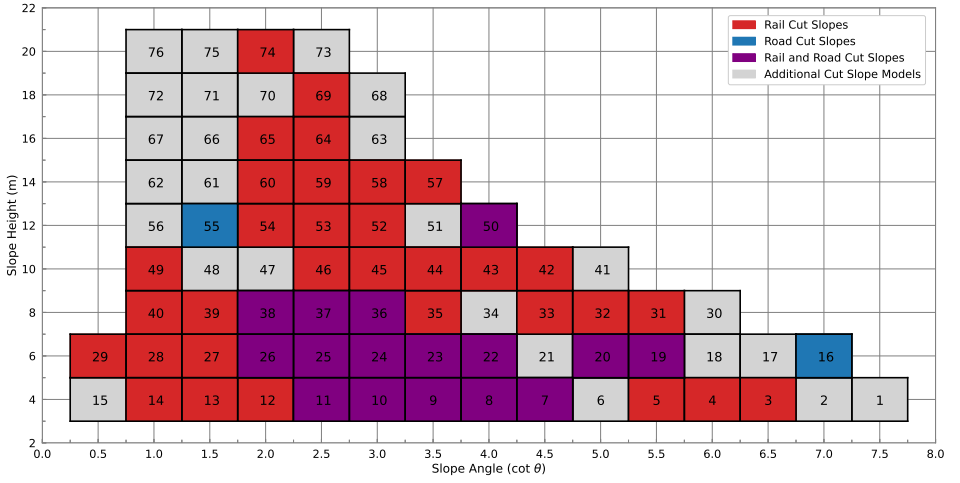

Figure S1 Identifiers of the computer experiments vs. slope height and angle cotangent used in the Latin hypercube design. This plot is consistent with the most commonly encountered geometries in the London-Bristol rail corridor (Network Rail, 2017).

Testing mean and correlation functions

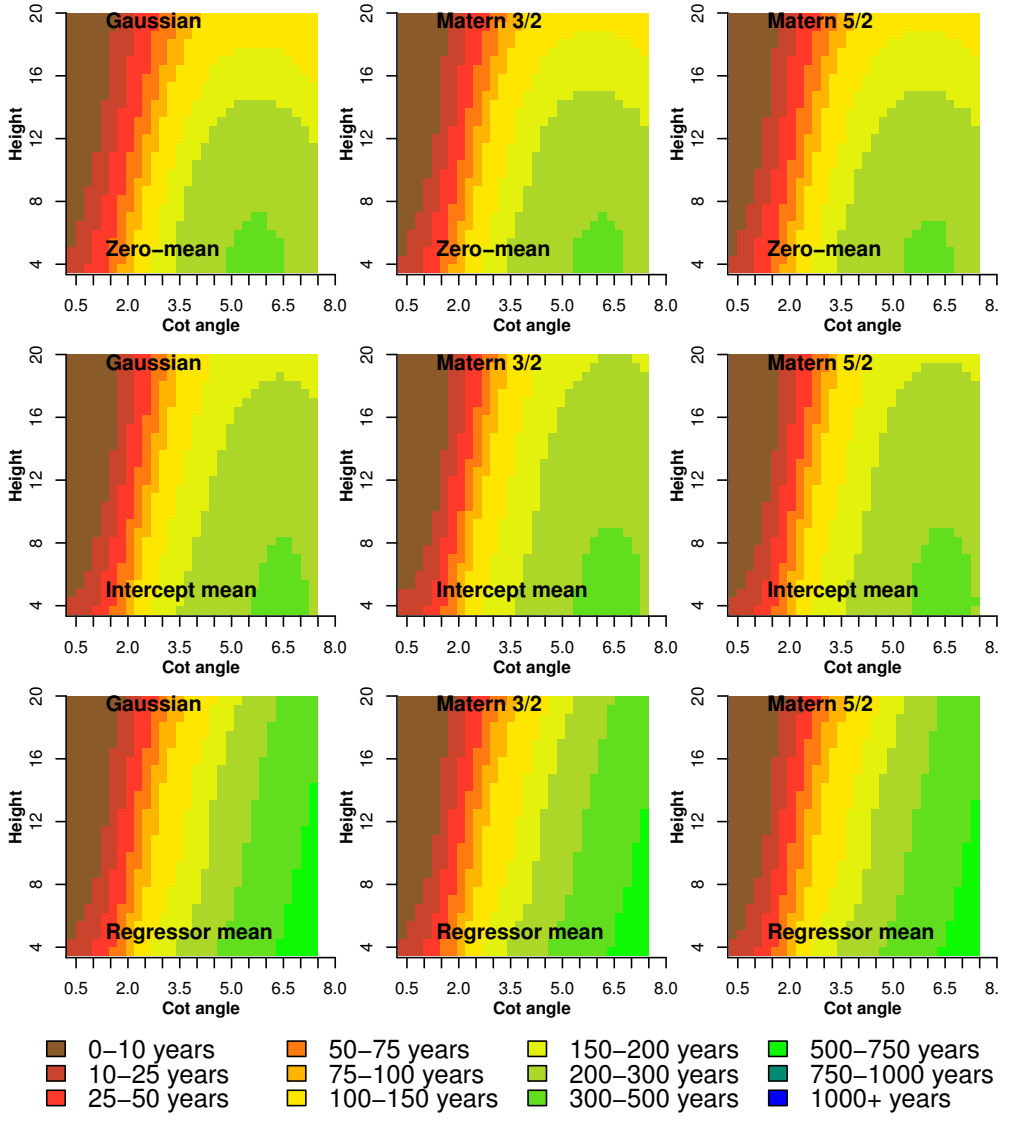

Figure S2 Time to failure maps versus slope geometry. Forms of the mean and correlation functions are indicated in the top and bottom left corners respectively. This Figure illustrates that the regressor mean function is most appropriate for our emulation problem, as the non-monotonic behaviour observed in the first two rows is not plausible to explain earthwork deterioration given fixed soil properties.

Output transformation validation

Different transformations of the TTF were tested in order to minimise predictive errors. A collection of set-aside validation runs were used to validate the GPE and identify the optimal output transformation. Figure S4 illustrates observed versus predicted TTFs for the validation data set. For the square root transformation, the predictions were made with Gaussian (C_G), Matern 3/2 ($C_{M,3/2}$) and Matern 5/2 ($C_{M,5/2}$) correlation functions, in the remaining cased $C_{M,3/2}$ was used. The square root transformation performs best in terms of MSE and R^2, with the $C_{M,5/2}$ correlation function giving the most optimal values. Thus, the square root transformation with the $C_{M,5/2}$ was chosen for further use. The remaining transformations perform less optimally with the natural logarithm transformation having the poorest performance as judged by R^2 and MSE.

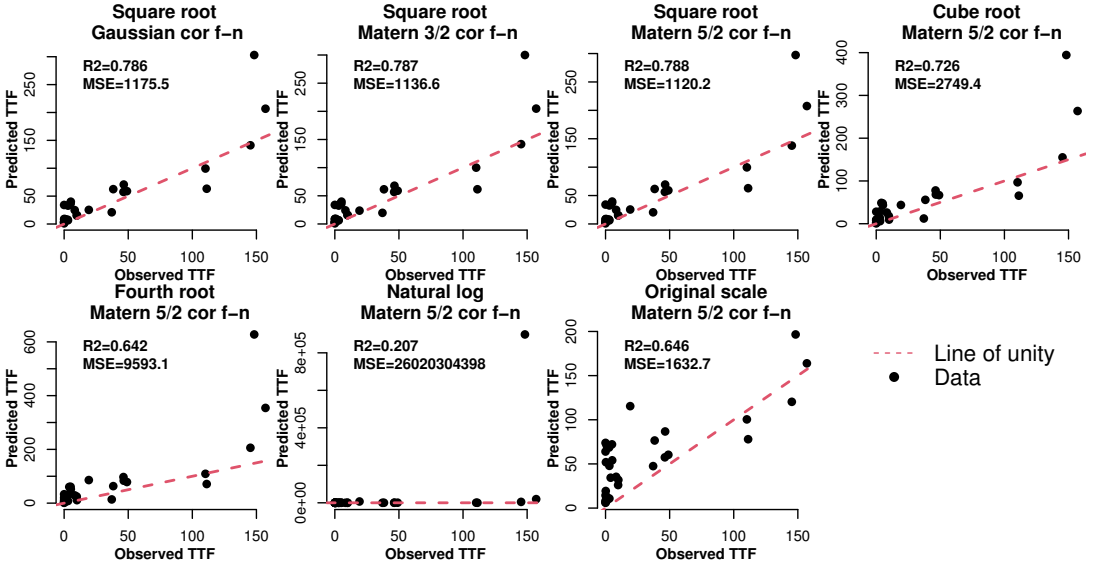

Figure S3 Predicted versus observed TTF for set-aside experiments. Coefficient of determination (R^2) and mean squared error (MSE) are shown in the top left corner of the of the plots. The red dashed line indicates equality between observed and predicted TTF.

Additional figures

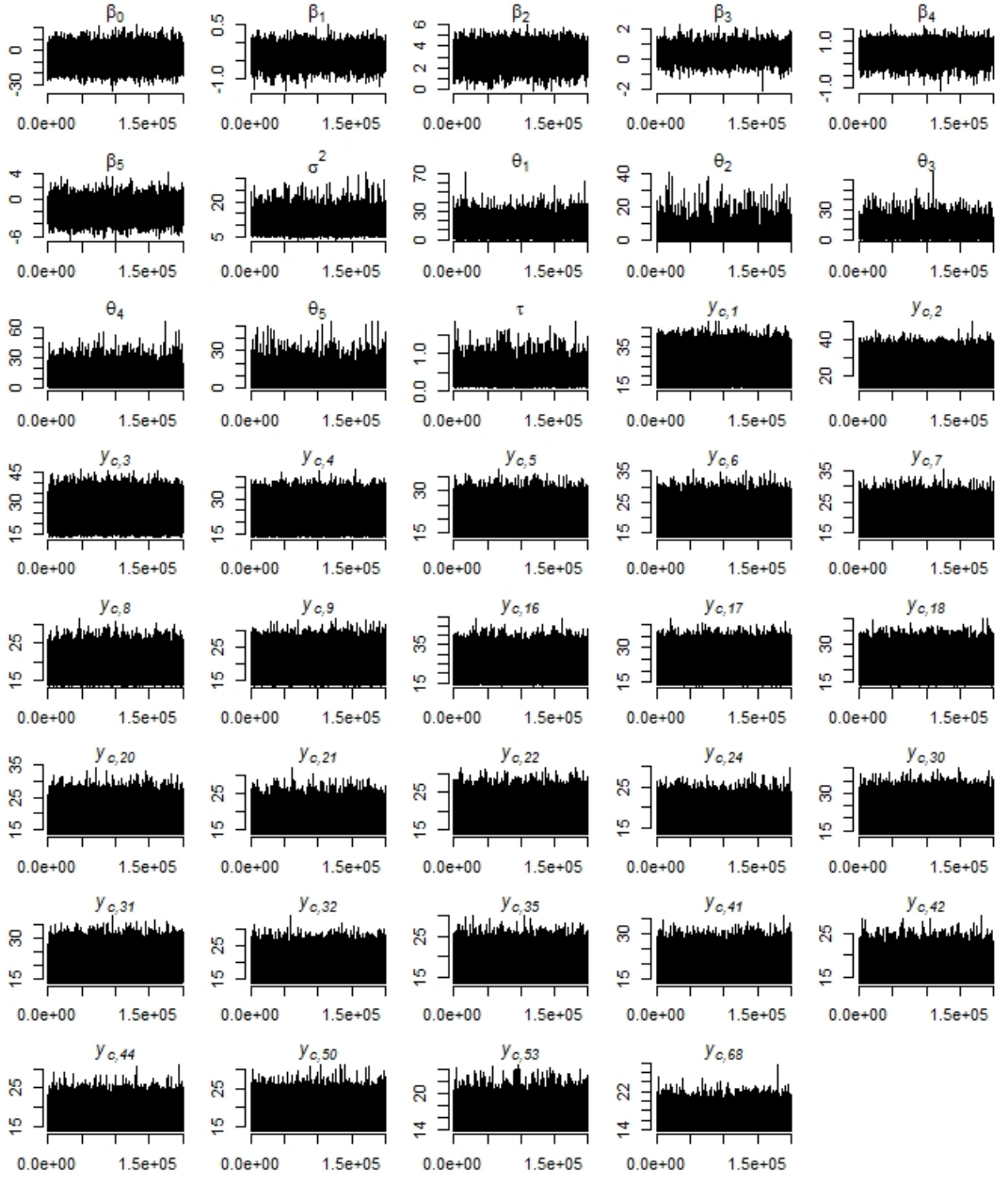

Figure S4 Trace plots of the posterior draws of the GPE model. All of the plots illustrate good exploration of the sample space. Most efficient mixing is observed for the censored values y_c.

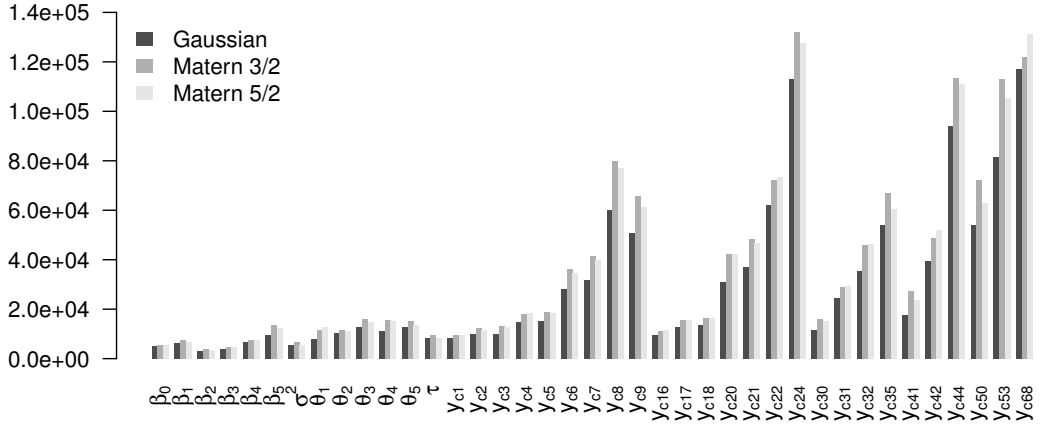

Figure S5 Effective sample size (ESS) of the posterior draws of the Gaussian process emulator. All of the ESS values are above 3000 illustrating good mixing. The largest ESS are observed for the censored values y_c indicating a lack of posterior autocorrelation. Using the Matern correlation function familiy appears to give the best efficiency.

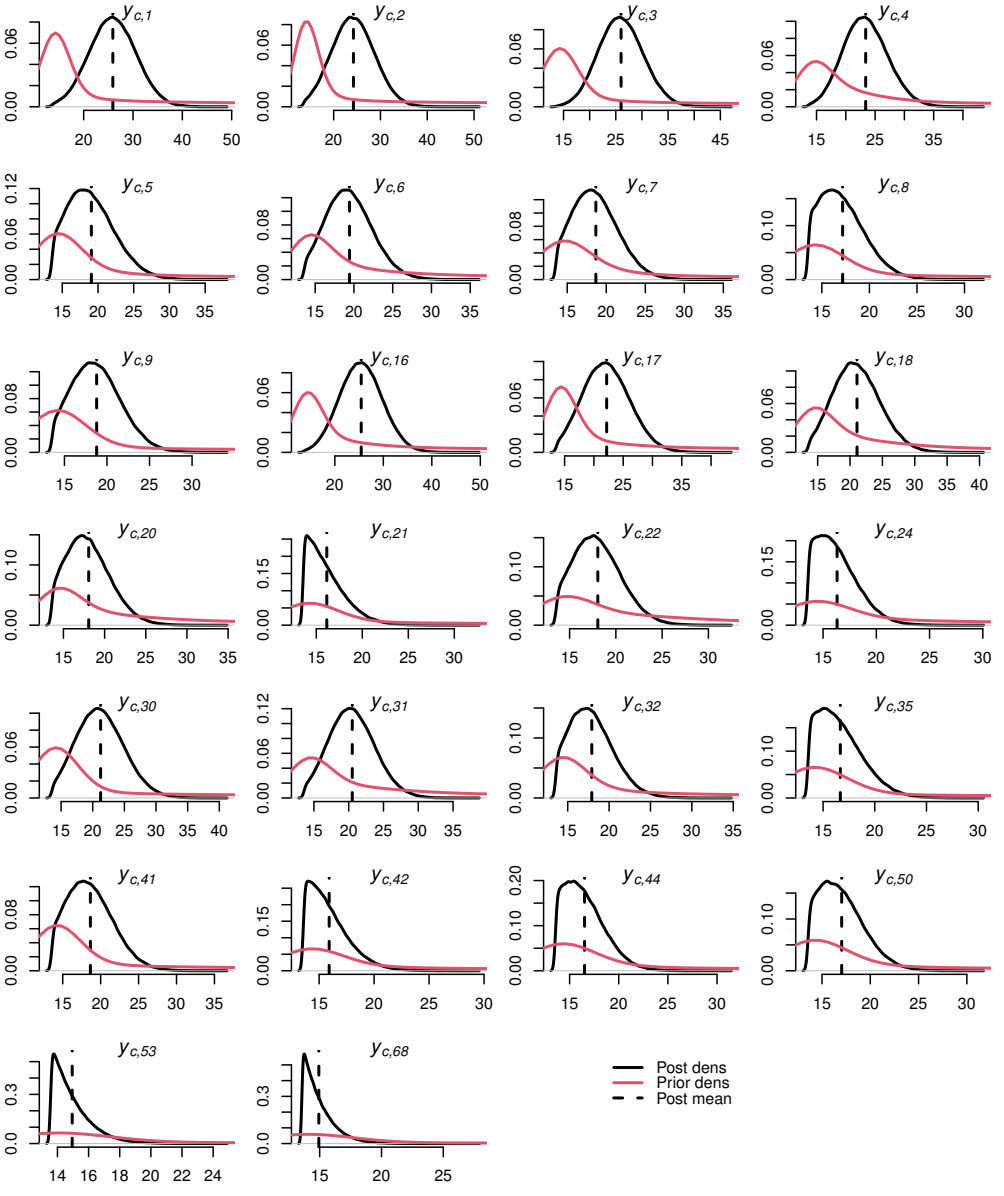

Figure S6 Density plots of the posterior draws of the GPE model of the censored values. The grestest reduction in variance compared to that of the prior distribution can be observed for the censored values whose posterior mean is close to the censoring limit of $\sqrt{184} = 13.6$. Otherwise, the posterior variance is close to or greater than the prior variance.

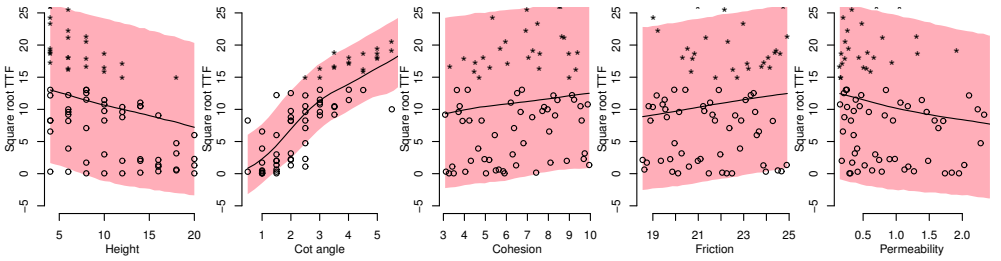

Figure S7 Posterior predictive (marginal) distributions of the GPE. Empty circles are the training data and the starts correspond to the posterior mean values of the censored observations. The red shaded region is the 95% marginal predictive interval and the black lines are the marginal mean behaviour. Both, the mean behaviour and the intervals capture all of the data and the poterior means of the censored values well.

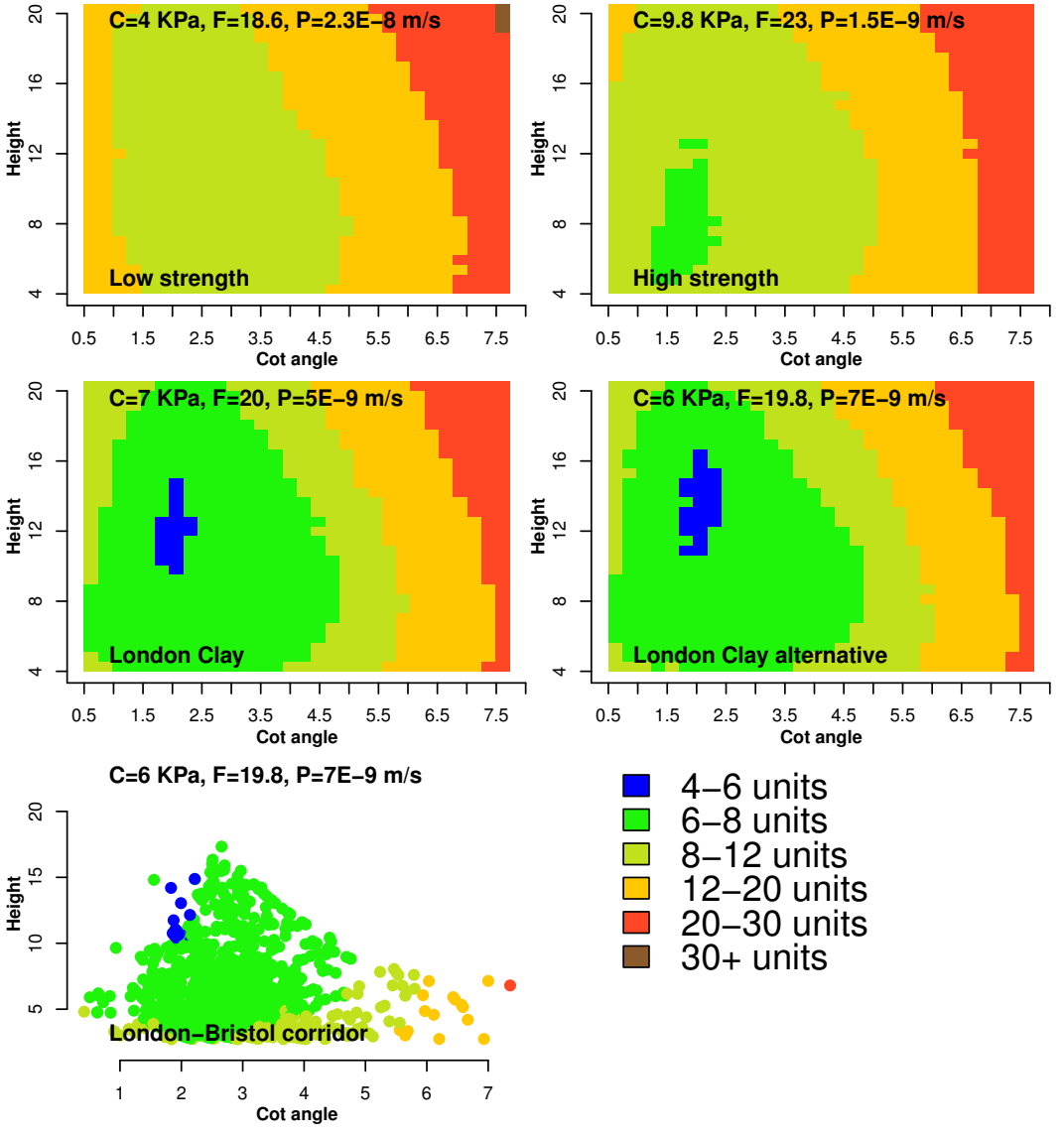

Figure S8 Posterior predictive variance maps. Cohesion kPa (C), friction angle (F) and permeability m/s (P) are fixed for every scenario and shown in the top left. The posterior variance is minimised away from the boundaries of our Latin hypercube design, e.g. for London Clay-type soil properties and moderately-stable (angle cotangent between 1.5 and 2.5) cutting slope geometries.